

Performance optimization of a SERF atomic magnetometer based on flat-top light beam

Ziqi Yuan(袁子琪),Junjian Tang(唐钧剑),Shudong Lin(林树东),andYueyang Zhai(翟跃阳),

Citation: Chin. Phys. B, 2024, 33 (**6**): 060703. DOI: 10.1088/1674-1056/ad401b
Journal homepage: http://cpb.iphy.ac.cn; http://iopscience.iop.org/cpb

What follows is a list of articles you may be interested in

Response optimization of a three-axis sensitive SERF magnetometer for closed-loop operation

Yuanrui Zhou(周原锐), Yongze Sun(孙永泽), Xixi Wang(汪茜茜), Jianan Qin(秦佳男), Xue Zhang(张雪), and Yanzhang Wang(王言章)
Chin. Phys. B, 2024, 33 (**2**): 020701. DOI: 10.1088/1674-1056/ad0b00

Suppression of laser power error in a miniaturized atomic co-magnetometer based on split ratio optimization

Wei-Jia Zhang(张伟佳), Wen-Feng Fan(范文峰), Shi-Miao Fan(范时秒), and Wei Quan(全伟)
Chin. Phys. B, 2023, 32 (**3**): 030701. DOI: 10.1088/1674-1056/ac81b1

A synthetic optically pumped gradiometer for magnetocardiography measurements

Shu-Lin Zhang(张树林), Ning Cao(曹宁)
Chin. Phys. B, 2020, 29 (**4**): 040702. DOI: 10.1088/1674-1056/ab7801

Miniature quad-channel spin-exchange relaxation-free magnetometer for magnetoencephalography

Jian-Jun Li(李建军), Peng-Cheng Du(杜鹏程), Ji-Qing Fu(伏吉庆), Xu-Tong Wang(王旭桐), Qing Zhou(周庆), Ru-Quan Wang(王如泉)
Chin. Phys. B, 2019, 28 (**4**): 040703. DOI: 10.1088/1674-1056/28/4/040703

A dual-axis, high-sensitivity atomic magnetometer

Rujie Li(李茹杰), Wei Quan(全伟), Wenfeng Fan(范文峰), Li Xing(邢力), Zhuo Wang(王卓), Yueyang Zhai(翟跃阳), Jiancheng Fang(房建成)
Chin. Phys. B, 2017, 26 (**12**): 120702. DOI: 10.1088/1674-1056/26/12/120702

Performance optimization of a SERF atomic magnetometer based on flat-top light beam

Ziqi Yuan(袁子琪)[1], Junjian Tang(唐钧剑)[1,2,†], Shudong Lin(林树东)[1], and Yueyang Zhai(翟跃阳)[1,2,3]

[1] *Key Laboratory of Ultra-Weak Magnetic Field Measurement Technology, Ministry of Education, School of Instrumentation and Optoelectronic Engineering, Beihang University, Beijing* 100191, *China*
[2] *School of Physics, Beihang University, Beijing* 100191, *China*
[3] *Hefei National Laboratory, Hefei* 230088, *China*

(Received 4 March 2024; revised manuscript received 12 April 2024; accepted manuscript online 18 April 2024)

We explore the impact of pumping beams with different transverse intensity profiles on the performance of the spin-exchange relaxation-free (SERF) atomic magnetometers (AMs). We conduct experiments comparing the traditional Gaussian optically-pumped AM with that utilizing the flat-top optically-pumped (FTOP) method. Our findings reveal that the FTOP-based approach outperforms the conventional method, exhibiting a larger response, a narrower magnetic resonance linewidth, and a superior low-frequency noise performance. Specifically, the use of FTOP method leads to a 16% enhancement in average sensitivity within 1 Hz–30 Hz frequency range. Our research emphasizes the significance of achieving transverse polarization uniformity in AMs, providing insights for future optimization efforts and sensitivity improvements in miniaturized magnetometers.

Keywords: atomic magnetometer (AM), spin-exchange relaxation-free (SERF), flat-top light beam, performance optimization

PACS: 07.55.Ge, 07.07.Df, 33.80.–b **DOI:** 10.1088/1674-1056/ad401b

1. Introduction

The precise measurement of weak magnetic fields finds broad applications in fundamental physics exploration and engineering.[1–3] As one of the most promising methods, the atomic magnetometer (AM) has attracted widespread attention in scientific research.[4–6] Notably, the spin-exchange relaxation-free (SERF) magnetometer has become the record holder for the highest sensitivity in magnetic field measurements due to its effective prolongation of the coherent time of the atomic ensemble.[7–9] Currently, SERF magnetometers have transitioned from laboratory settings to practical applications such as magnetocardiography (MCG) and magnetoencephalography (MEG).[10–14] They are also expected to play a crucial role in advancing frontier scientific fields such as dark matter exploration and the search for charge-parity-time violation, etc.[15,16] The most classic configuration of SERF AMs involves a dual-beam configuration with orthogonal pump and probe light. Alkali metal atoms are pumped using circularly polarized light, while the atomic spin rotation induced by an external magnetic field is detected using linearly polarized light.[17,18] Based on this configuration, Dang *et al.* achieved a magnetic field sensitivity of 0.16 fT·Hz$^{-1/2}$ in a gradiometer configuration with a measurement volume of 0.45 cm^3 in 2010.[19] To date, numerous researchers continue their efforts to enhance the performance of SERF magnetometers.

The optimization of SERF magnetometer performance mainly revolves adjusting parameters like gas pressure,[20] temperature,[21] pump beam intensity and frequency,[22] probe beam intensity, frequency,[23] and other relevant factors. Once the operating parameters of the atomic vapor cell are determined, the most important aspect affecting the magnetometer's performance is the steady-state spin polarization (P_z) of the atomic ensemble. Typically, the magnetometer achieves the optimal performance when $P_z = 0.5$. However, factors such as laser profile, magnetic field gradient, and temperature gradient impact the spatial uniformity of polarization, preventing the magnetometer from reaching its theoretical optimum. Existing approaches for enhancing polarization uniformity primarily address longitudinal nonuniformity caused by atomic absorption. Methods to improve the longitudinal polarization uniformity of the atomic ensemble involve techniques like beam reflection[24] and opposite pumping.[25,26] Nevertheless, improving transverse polarization uniformity proves challenging through direct alterations to the magnetometer configuration, as it mainly depends on the transverse intensity distribution of the pump light. The adoption of a flat-top beam proves to be a feasible approach for enhancing the uniformity of transverse polarization. This method has found application in various fields such as atomic co-magnetometer,[27] Rydberg atomic sensing,[28] and electromagnetic induction transparency effect.[29] Common techniques for generating the flat-top beam include the use of diffractive optical element (DOE),[30] spatial light modulator (SLM),[31] acousto–optical deflector,[32] aspherical lens,[33] and optical metasurface.[34]

†Corresponding author. E-mail: tangjunjian@buaa.edu.cn

© 2024 Chinese Physical Society and IOP Publishing Ltd

However, the application of flat-top light has rarely been studied for ultra-sensitive SERF AMs.

In this paper, we explore the application of flat-top optically-pumped (FTOP) method in SERF AM and analyze its impact on the performance optimization of dual-beam AM. The FTOP method ensures uniform spin polarization along different positions on the probe path and enables complete compensation of residual magnetic fields. Our findings demonstrate that FTOP AM displays a larger response, a narrower magnetic resonance linewidth and better low frequency noise performance compared to the Gaussian optically-pumped (GOP) AM at the same optical power density. Therefore, we demonstrate that enhancing the uniformity of the transverse polarization of the atomic vapor cell emerges as an important aspect for optimizing the magnetometer's performance.

2. Theoretical analysis

In AMs, the variation in atomic spins reflects the external magnetic fields. When the atomic density is sufficiently high under near-zero magnetic fields, the atomic ensemble will reach the SERF regime. Under such conditions, the evolution of atomic spins described by the complicated density matrix can be approximated by the Bloch equations. When the diffusion term is ignored and the circularly polarized pump beam is set along the z-axis, the electron spin polarization vector $\boldsymbol{P}$ can be expressed as[35]

$$q\frac{\mathrm{d}\boldsymbol{P}}{\mathrm{d}t}=\boldsymbol{\Omega}(t)\times\boldsymbol{P}+R_{\mathrm{op}}\hat{z}-\Gamma'\boldsymbol{P}, \tag{1}$$

where q is the nuclear slowing down factor of ^{87}Rb, $\boldsymbol{\Omega}(t)=\gamma\boldsymbol{B}(t)$ is the angular frequency of atomic Larmor precession about the external magnetic field $\boldsymbol{B}(t)$, γ is the gyromagnetic ratio, $\Gamma'=R_{\mathrm{op}}+\Gamma$, R_{op} is the optical pumping rate, Γ is the relaxation rate mainly contributed by collisions with the glass cell wall, diffusion of atoms and spin destruction collisions, and $\hat{z}$ represents the direction of the circularly polarized pumping beam. The steady state solution of Eq. (1) is

$$\boldsymbol{P}=\frac{R_{\mathrm{op}}}{\Gamma'\left(\Gamma'^2+\Omega_x^2+\Omega_y^2+\Omega_z^2\right)}\begin{cases}\Gamma'\Omega_y+\Omega_x\Omega_z\\ -\Gamma'\Omega_x+\Omega_y\Omega_z\\ \Gamma'^2+\Omega_z^2\end{cases}. \tag{2}$$

As for the dual-beam configuration, the linearly polarized probe is sensitive to variations in P_y, a parameter closely related to the magnitude of B_x. For the D2 transition, the changes in atomic spin orientation give rise to a Faraday rotation in the polarization of the probe beam, expressed as

$$\varphi=\frac{1}{4}ln_{\mathrm{Rb}}r_{\mathrm{e}}f_{\mathrm{D2}}c\mathrm{Im}\left[V(\Delta\nu)\right]P_y, \tag{3}$$

where l is the effective propagation length of the probe beam, n_{Rb} is the density of the alkali vapor, r_{e} is the classical electron radius, f_{D2} is the oscillator strength, c is the speed of light, $\Delta\nu$ is the laser detuning from the D2 transition. Equation (3) gives a dispersion response as a function of B_x with a maximum slope obtained when $R_{\mathrm{op}}=\Gamma=1/2\Gamma'$, giving the spin polarization $P_z=1/2$.

The SERF magnetometer response model discussed above ignores the impact of spatial variations in laser profiles. In fact, the measured rotation angle is the integral of the response at each position in the cell. In our experiment, the pump light spot (with the diameter of 7 mm) can cover almost the entire vapor cell, while the diameter of the probe light spot is only 1 mm. Therefore, we ignore the effect of the spatial distribution of the probe beam on the performance of the AM, and only consider the effect of the transverse distribution of the pump beam. Since the pumping rate R_{op} is proportional to the intensity of the pump light, it can be considered that the spatial distribution of R_{op} is determined by the spatial distribution of the laser intensity. If Eq. (3) is utilized to estimate the noise limit of the magnetometer system without accounting for the spatial distribution of R_{op}, the resulting value will be lower than experimental measurements.

To analyze how the spatial dependence of pump laser profiles affects the magnetometer's performance, we give a differential and position dependent version of the rotation per unit field as

$$\frac{\partial\left(\dfrac{\varphi}{B_x}\right)}{\partial y}=\frac{1}{4}ln_{\mathrm{Rb}}r_{\mathrm{e}}f_{\mathrm{D2}}c\mathrm{Im}\left[V(\Delta\nu)\right]\times\frac{\gamma R_{\mathrm{op}}(x,y,z)}{\Gamma'(x,y,z)^2+\Omega_z(x,y,z)^2}. \tag{4}$$

Equation (4) is integrated along the propagation path of the probe beam to obtain the total rotation angle of the unit field

$$\frac{\varphi}{B_x}=\frac{1}{4}n_{\mathrm{Rb}}r_{\mathrm{e}}f_{\mathrm{D2}}c\mathrm{Im}\left[V(\Delta\nu)\right]\gamma\int_{-l/2}^{l/2}\frac{R_{\mathrm{op}}(y)}{\Gamma'(y)^2+\Omega_z(y)^2}\mathrm{d}y. \tag{5}$$

Since the magnetometer generally has the largest compensation error for the residual magnetic field of the pump axis due to the light shift, Ω_x and Ω_y are neglected in Eq. (5). Based on the working parameters of the vapor cell we used, the calculated diffusion distance is 0.3 mm, significantly smaller than the diameter of the pump light spot. Furthermore, since the atoms undergoing diffusion pumping remain unaffected by the light shift, we have neglected the decrease in polarization due to diffusion.

For the Gaussian pump beam, the spatial distribution of R_{op} along the probe path satisfies

$$R_{\mathrm{op}}(y)=R_{\mathrm{op}}^0\exp\left(-2\frac{y^2}{\omega_0^2}\right), \tag{6}$$

where $R_{\rm op}^0$ is the optical pumping rate at the center of the vapor cell ($y=0$), and ω_0 is the radius of the pump light spot. Combining Eq. (5) with Eq. (6), the distribution of $R_{\rm op}(y)$ that minimizes $\int_{-l/2}^{l/2}(R_{\rm op}(y)-\Gamma)\,{\rm d}y$ will yield the maximum magnetometer response. From this, the value of $R_{\rm op}^0$ can be determined. For flat-top light, the distribution of $R_{\rm op}$ is uniform, and the corresponding maximum response obtained can be expressed as

$$\frac{\varphi}{B_x}=\frac{\gamma}{16\Gamma}ln_{\rm Rb}r_{\rm e}f_{\rm D2}c{\rm Im}\left[V(\Delta\nu)\right]. \tag{7}$$

By substituting the experimental parameter values into Eqs. (5)–(7), the maximum total rotation angle per unit field achievable by Gaussian light pumping and flat-top light pumping can be obtained through numerical simulations. Since the pump light in our experiment is near-resonant, we neglect the influence of the light shift magnetic field ($\Omega_{\rm LS}$) in the comparative analysis of the optimal values for Gaussian light and flat-top light. That is, assume that B_z is completely compensated. Calculation results prove that, at the same operating temperature, compared to the Gaussian pump beam, flat-top light can achieve greater response and smaller linewidth.

The Gaussian distribution of the pump beam introduces inevitable inhomogeneity in the transverse polarization of the atomic ensemble. To ensure uniform optical pumping, sometimes the pump light may be detuned many linewidths from resonance. However, it will induce a significant transverse-dependent light shift, resulting in the inability to fully cancel B_z using a set of magnetic coils. The incomplete compensation of the residual magnetic field along the pumping axis and the non-uniform transverse polarization negatively impact the magnetometer's performance. In this scenario, the advantage of flat-top pumping will be more prominent, as the transverse uniformity achieved by the flat-top beam enables the full compensation of Ω_z, directly addressing these shortcomings. Simultaneously, it allows more atoms in the probe path to achieve the optimal working condition with $P_z=1/2$, effectively improving the performance of AMs.

3. Experimental setup

Figure 1 shows the experimental setup. Our experiment was operated in four layers of mu-metal shield to achieve the required weak magnetic field of several nT. An ^{87}Rb vapor cell with an internal dimension of $8\times8\times8$ mm filled with 600-Torr N_2 was placed in the center of the magnetic shield for sensing. To enable a larger diameter of pump light to be used, we designed a new oven structure, as shown in the inset of Fig. 1. The light transmission aperture of the pump path was set to 10 mm. In addition, to improve the thermal insulation of the oven and the heating efficiency, we glued two 12.7 mm diameter windows coated with 795 nm anti-reflection film outside the light transmission hole. A pair of magneto–electric heating films attached to the cell driven by a 200-kHz alternating current was used to heat the cell. The three-axis magnetic fields were applied by three pairs of Helmholtz coils driven by function generators. The residual magnetic fields in the two non-pumping axes could be decreased to tens of pT through precision magnetic compensation.

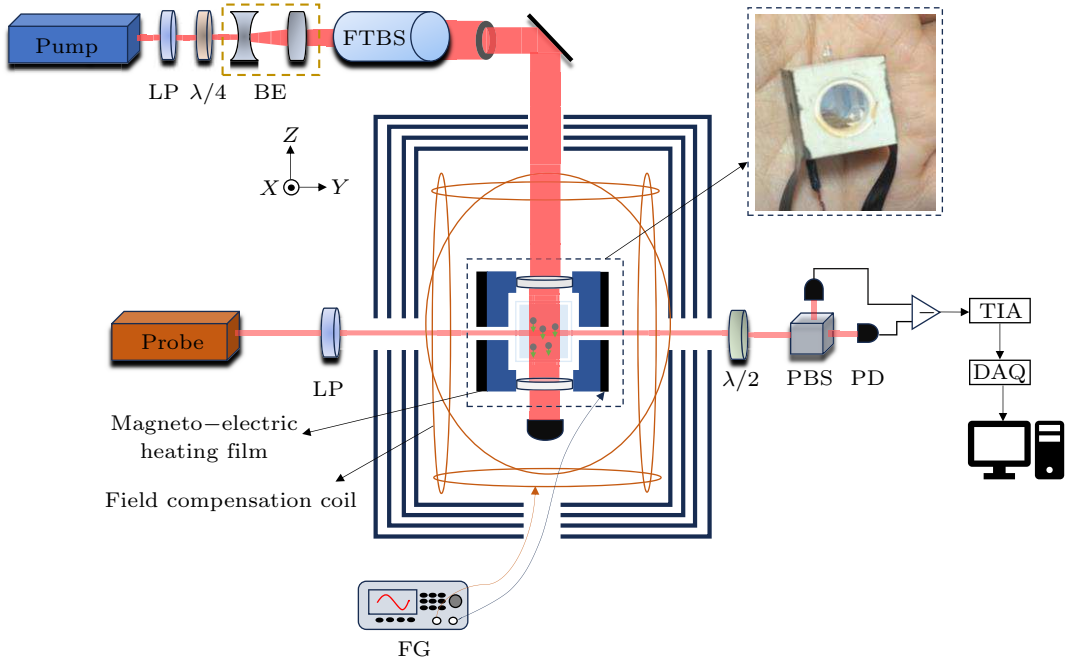


Fig. 1. Schematic diagram of our dual-beam SERF magnetometer. LP: linear polarizer, BE: beam expander, FG: function generator, TC: temperature controller, PBS: polarization beamsplitter, PD: photodetector, TIA: transimpedance amplifier, DAQ: data acquisition system, FTBS: flat-top beam shaper, $\lambda/4$: quarter-wave plate, $\lambda/2$: half-wave plate.

Our optical system contains the pump path and probe path. The pump light was generated by a distributed feedback (DFB) laser (laser tube type: EYP-DFB-0795-BFW01-0005) with a linewidth of narrower than 1 MHz. Its wavelength was adjusted to the near resonance transition center of the ^{87}Rb D1 line. After the linear polarizer (LP) and quarter-wave plate ($\lambda/4$), the pump light was converted to a circularly polarized light. The beam expander then expanded the Gaussian pump beam from approximately 1 mm diameter to 7 mm diameter. The flat-top beam shaper (FTBS) composed of an aspherical lens was used to convert the Gaussian beam into a flat-top beam with a diameter of about 15.2 mm. After FTBS, a circular aperture with a diameter of 7 mm was used to intercept the center part of the flat-top beam to keep it the same diameter as the Gaussian beam in the experiment. Ultimately, the used Gaussian beam or flat-top beam both entered the vapor cell with a spot diameter of 7 mm. In our experiment, the wavelength and power of the probe light were adjusted to optimize the magnetometer's response. The probe light was generated using a distributed Bragg reflector (DBR) laser (laser tube type: PH780DBR180TS), with its frequency shifted to be blue-detuned by 120 GHz from the transition center of the ^{87}Rb D2 line. After the LP, the probe beam was converted to linearly polarized light with a spot diameter of 1 mm and an intensity of approximately 2 mW before entering the vapor cell. We detected the probe signal via balanced polarimetry consisting of a half-wave plate ($\lambda/2$), a polarization beamsplitter (PBS), and two photodetectors (PDs).

We employed a temperature control system with the precision of 0.02 K. The probe signal was collected by photodetectors (Hamamatsu S13957-01). After this, the signal was converted and amplified by a transimpedance amplifier (TIA) and collected using the PXIe-4464 module (National Instruments).

4. Measurement results

Figure 2 displays two-dimensional images illustrating the transverse intensity distribution of both the Gaussian pump light and flat-top pump light. Additionally, it presents the intensity distribution ratios at various positions along the x and y axes. Evidently, the transverse intensity distribution of the flat-top light exhibits better uniformity.

To demonstrate the optimization effect of flat-top optical pumping on AM performance, we conducted tests on the magnetometer at different temperatures and optical power conditions. Following each parameter adjustment, the precision magnetic compensation process was carried out. Under different working conditions, the AM response curve was obtained after scanning the magnetic field along the sensitive axis. Figures 3 and 4 depict the response curves under Gaussian pump light and flat-top pump light, respectively. The optical power range was adjusted differently under various temperatures, as the optical depth of the cell deepens with higher temperatures, necessitating greater optical power.

As shown in Figs. 3 and 4, the response curves maintain a dispersion-like pattern of zero-field resonance within the appropriate parameter range, featuring a linear response region sensitive to external magnetic fields. However, Fig. 3(c) reveals that the inhomogeneity nature of Gaussian pump light makes the Lorentzian dispersion curve unsuitable for describing the magnetometer response under conditions of high atomic density and pumping rate. This is because the increase of atomic density and pumping rate further worsens the inhomogeneity of the transverse polarization, making the integral response of atoms at different positions along the probe path unsuitable for representation through a Lorentzian dispersion curve. Subsequently, we extract the response scale factors and magnetic linewidths of Gaussian and flat-top beams under various operating parameters from Figs. 3 and 4, as shown in Figs. 5(a) and 5(c), and 5(b) and 5(d), respectively. The corresponding datasets are presented in Tables 1 and 2 for clear comparison.

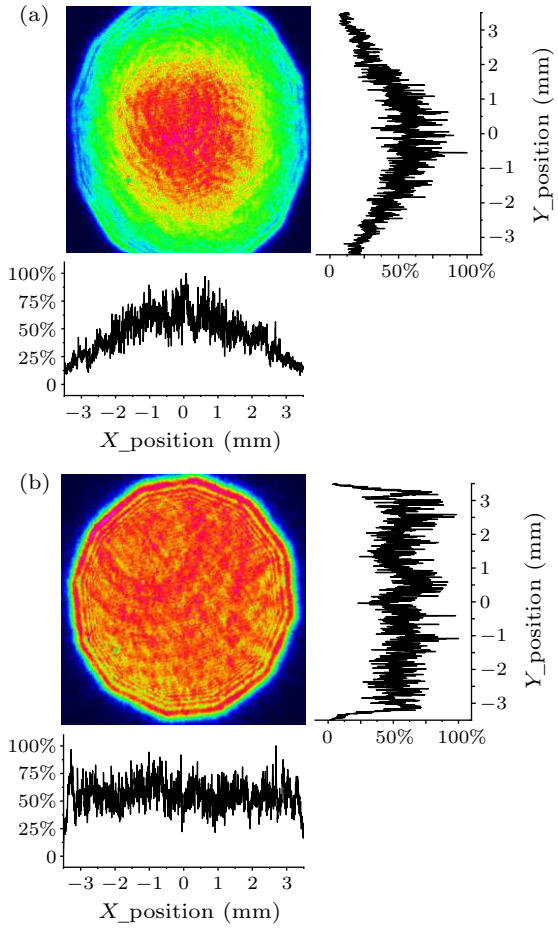


Fig. 2. The two-dimensional intensity profiles and the transverse intensity distribution ratios of the (a) Gaussian beam and (b) flat-top beam. The 4-sigma diameters of the two beams are both 7 mm.

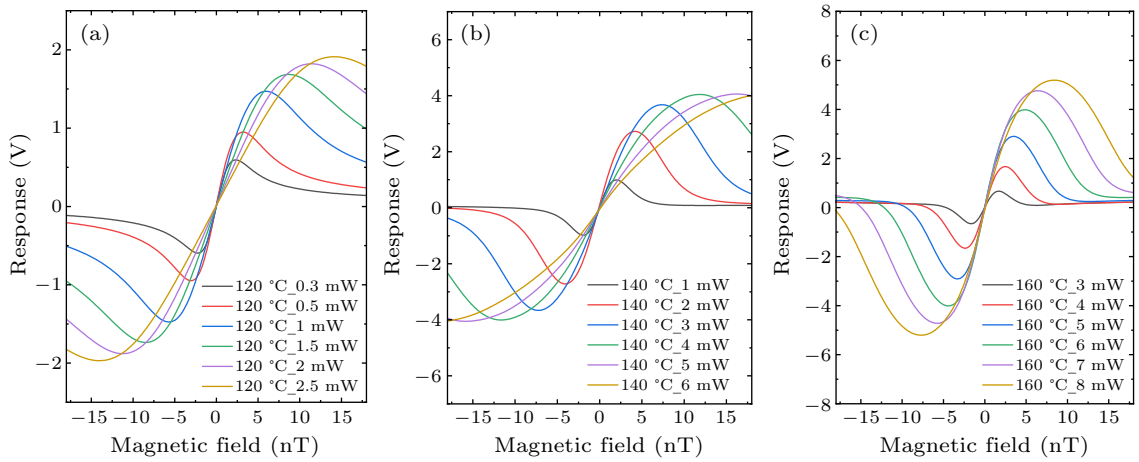


Fig. 3. Response curves under different temperatures and optical powers of the pump light in a Gaussian beam configuration. The magnetic field scanning range along the sensitive axis spans approximately −20 nT to 20 nT.

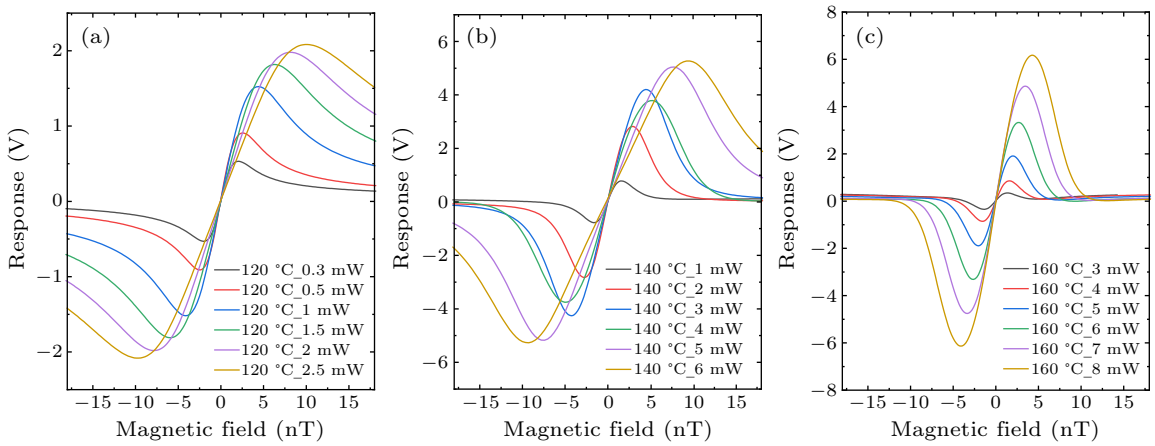


Fig. 4. Response curves under different temperatures and optical powers of the pump light in a flat-top beam configuration. The magnetic field scanning range along the sensitive axis spans approximately −20 nT to 20 nT.

Table 1. Comparison of optimal scale factors attained through the GOP method and the FTOP method at different temperatures.

Temperature (°C)	Scale factor of GOP method (V/nT)	Scale factor of FTOP method (V/nT)
120	0.53	0.63
130	0.95	1.07
140	1.11	1.58
150	1.52	1.75
160	1.66	2.32

Table 2. Comparison of linewidths between the GOP method and the FTOP method when optimal scale factors are achieved at different temperatures.

Temperature (°C)	Linewidth of GOP method (nT)	Linewidth of FTOP method (nT)
120	6.11	5.00
130	6.85	5.00
140	7.32	5.93
150	7.04	6.85
160	9.26	8.33

Analysis of Fig. 5 reveals that the response scale factors and magnetic linewidths of two types of AMs, namely GOP and FTOP, exhibit similar trends concerning temperature and incident light intensity. Specifically, the magnetic linewidth $\Delta\omega$ is defined as $\Delta\omega = (R_{\rm op} + \Gamma)/q$, where $R_{\rm op}$ increases with higher light intensity, and Γ decreases with rising temperature. Consequently, $\Delta\omega$ decreases with increasing temperature and increases with incident intensity. In addition, under the same temperature conditions, the magnetometer response initially increases and then decreases with an increase in optical power. At the point of maximum response, the magnetometer is considered to be in a state where $R_{\rm op} = \Gamma$. As temperature increases, the absorption of pump light in the atomic cell rises, leading to an overall reduction in the pumping rate. This causes the maximum response point to move towards higher light power at higher temperatures. Notably, when comparing the response scale factor and linewidth of GOP and FTOP across various parameters, it becomes evident that the FTOP AM exhibits a narrower linewidth and a larger response scale factor under identical working conditions. According to the sensitivity definition formula,[7] a magnetometer with a narrower linewidth can achieve higher fundamental sensitivity, and an increased response scale factor contributes to an improved signal-to-noise ratio. Therefore, theoretically, the FTOP AM has the potential to achieve higher sensitivity.

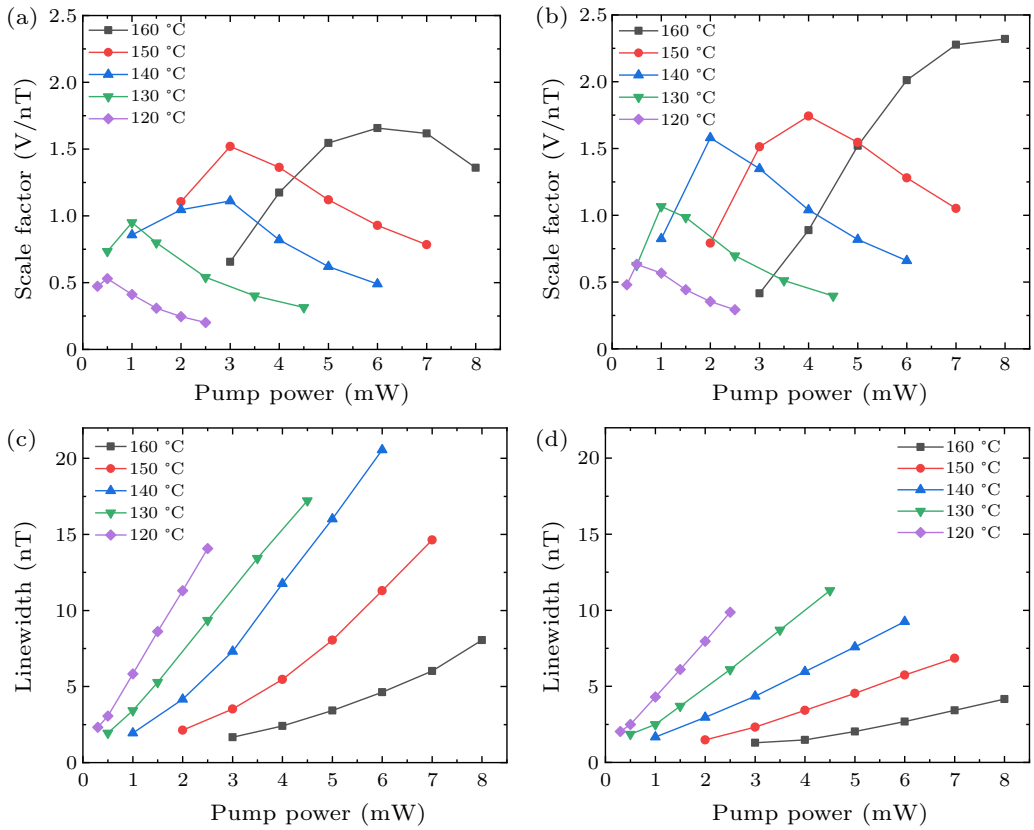


Fig. 5. Response scale factors and magnetic linewidths of (a) and (c) Gaussian beam and (b) and (d) flat-top beam under different operating parameters. The values are derived from Figs. 3 and 4.

For a comparative evaluation of the magnetic field sensitivity between these two configurations, a calibration signal with a frequency of 30.5 Hz and an amplitude of 100 pTrms was generated along the *x*-axis. Response signals were continuously collected for 50 s and then transformed and calculated by fast Fourier transform to obtain averaged power spectral density values. Sensitivities were determined by dividing the power spectral density values by their corresponding frequency responses. As an illustrative example, we present the sensitivities of GOP and FTOP AMs under conditions of 140 °C and 3 mW in Fig. 6. The FTOP AM exhibits a notable sensitivity advantage over the GOP AM, particularly in the low frequency band. This feature enables the FTOP AM to reach a universally better sensitivity under different experimental conditions. Average sensitivity values across the frequency range from 1 Hz to 30 Hz under other experimental conditions are provided in Table 3. In the best-case scenario for both configurations, the average sensitivity of FTOP AM@1–30 Hz can be improved by 16% (from 9.20 fT·Hz$^{-1/2}$ to 7.74 fT·Hz$^{-1/2}$) compared to GOP AM. The primary limitation to sensitivity improvement lies in the intrinsic magnetic noise of the magnetic shield, which can be further suppressed by incorporating a ferrite shield. The suppression of magnetic noise may further highlight the sensitivity advantage of the FTOP method, and make a breakthrough in the limit sensitivity.

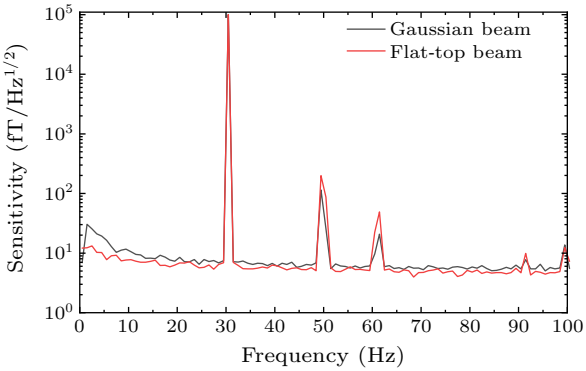


Fig. 6. Magnetic field sensitivity spectra of the two detection methods. The noise peak at 50 Hz is the power frequency noise, and the rest is the high-order resonances of the calibration signal.

Table 3. Comparison of average sensitivity @1–30 Hz between Gaussian beam and flat-top beam.

Temperature (°C)	120				140				160			
Pump intensity (mW)	0.5		1		2		3		5		6.5	
Gaussian (G)/flat-top (F)	G	F	G	F	G	F	G	F	G	F	G	F
Sensitivity (fT·Hz$^{-1/2}$)	11.10	9.42	13.40	11.36	9.20	8.08	12.39	7.74	10.56	8.69	10.95	9.11

5. Conclusion and perspectives

We have conducted theoretical and experimental investigations on two pumping methods, GOP and FTOP, in dual-beam AMs. We prove that FTOP effectively addresses the limitations of GOP, enhancing the overall performance of AM. Specifically, FTOP proves superior in the transverse polarization uniformity of the atomic ensemble. This improvement is evident in the increased response scale factor, reduced linewidth, and enhanced sensitivity. In situations where frequency shift cannot be avoided, flat-top optical pumping can fully compensate for the residual magnetic field along the pumping axis and eliminate the impact of position-dependent frequency shift on the performance of AMs.

Our study highlights the significance of the transverse distribution of pump light, aiding in the enhancement of pump light utilization efficiency and improving the performance of AMs under identical optical power density conditions. Therefore, the FTOP method can be expected to further improve the performance of miniaturized and arrayed AMs in the future on the basis of the miniaturization and integration of the beam shaping method.

Acknowledgments

Project supported by the National Natural Science Foundation of China (Grant No. 62303029), the China Postdoctoral Science Foundation (Grant No. 2022M720364), and the Innovation Program for Quantum Science and Technology (Grant Nos. 2021ZD0300500 and 2021ZD0300503).

References

[1] Aslam N, Zhou H Y, Urbach E K, Turner M J, Walsworth R L, Lukin M D and Park H 2023 *Nat. Rev. Phys.* **5** 157
[2] Shah V, Knappe S, Schwindt P D D and Kitching J 2007 *Nat. Photonics* **1** 649
[3] Jiang M, Su H W, Garcon A, Peng X H and Budker D 2021 *Nat. Phys.* **17** 1402
[4] Qu W Z, Jin S C, Sun J, Jiang L, Wen J M and Xiao Y 2020 *Nat. Commun.* **11** 1752
[5] Zhang R, Xiao W, Ding Y D, Feng Y L, Peng X, Shen L, Sun C X, Wu T, Wu Y L, Yang Y C, Zheng Z Y, Zhang X Z, Chen J B and Guo H 2020 *Sci. Adv.* **6** eaba8792
[6] Lin S D, Tang J J, Yuan Z Q, Huang B Y, Wang Y H and Zhai Y Y 2023 *Appl. Phys. Lett.* **123** 194001
[7] Kominis I K, Kornack T W, Allred J C and Romalis M V 2003 *Nature* **422** 596
[8] Tang J J, Zhai Y Y, Zhou B Q, Han B C and Liu G 2021 *IEEE Trans. Instrum. Meas.* **70** 1504808
[9] Boto E, Holmes N, Leggett J, Roberts G, Shah V, Meyer S S, Muñoz L D, Mullinger K J, Tierney T M, Bestmann S, Barnes G R, Bowtell R and Brooks M J 2018 *Nature* **555** 657
[10] Yuan Z Q, Liu Y, Xiang M, Gao Y, Suo Y C, Ye M and Zhai Y Y 2023 *Opt. Laser Technol.* **164** 109534
[11] Nardelli N V, Perry A R, Krzyzewski S P and Knappe S A 2020 *EPJ Quantum Technol.* **7** 11
[12] Guo Q Q, Hu T, Feng X Y, Zhang M K, Chen C Q, Zhang X, Yao Z K, Xu J Y, Wang Q and Fu F Y 2023 *Chin. Phys. B* **32** 040702
[13] Boto E, Seedat Z A, Holmes N, Leggett J, Hill R M, Roberts G, Shah V, Fromhold T M, Mullinger K J, Tierney T M, Barnes G R, Bowtell R and Brookes M J 2019 *NeuroImage* **201** 116099
[14] Yuan Z Q, Lin S D, Liu Y, Tang J J, Long T Y and Zhai Y Y 2024 *iScience* **27** 109250
[15] Safronova M S, Budker D, DeMille D and Kimball D F J 2018 *Rev. Mod. Phys.* **90** 025008
[16] Brown J M, Smullin S J, Kornack T W and Romalis M V 2010 *Phys. Rev. Lett.* **105** 151604
[17] Tang J J, Liu Y, Wang Y X, Zhou B Q, Han B C, Zhai Y Y and Liu G 2022 *Appl. Phys. Lett.* **120** 084001
[18] Lin S D, Tang J J, Yuan Z Q, Cao L and Zhai Y Y 2023 *IEEE Trans. Instrum. Meas.* **73** 1500410
[19] Dang H B, Maloof A C and Romalis M V 2010 *Appl. Phys. Lett.* **97** 151110
[20] Wang Y X, Jin G, Tang J J, Zhou W Y, Han B C, Zhou B Q and Shi T 2022 *Opt. Express* **30** 336
[21] Zhang S W, Lu J X, Ye M, Zhou Y, Yin K F, Lu F, Yan Y G and Zhai Y Y 2022 *IEEE Trans. Instrum. Meas.* **71** 1
[22] Tang J J, Zhai Y Y, Cao L, Zhang Y H, Li L, Zhao B B, Zhou B Q, Liu G and Han B C 2021 *Opt. Express* **29** 15641
[23] Xing B Z, Sun C, Liu Z A, Zhao J P, Lu J X, Han B C and Ding M 2021 *Opt. Express* **29** 5055
[24] Cao L, Tang J J, Zhang Y H, Yuan Z Q, Li J J, Zhai Y Y and Liu Y 2023 *Sens. Actuator A Phys.* **353** 114247
[25] Zhao J P, Liu G, Lu J X, Ding M, Ma Y N, Ji J, Yang K, Ma D Y, Xing B Z, Zhang N, Sun C and Han B C 2020 *Meas. Sci. Technol.* **32** 035902
[26] Yao H, Maddox B and Renzoni F 2023 *Opt. Express* **31** 509
[27] Chen X, Fang X J, Ma D Y, Liu Y, Cao L and Zhai Y Y 2022 *Appl. Opt.* **61** C55
[28] Wang Z, Jing M Y, Zhang P, Yuan S X, Zhang H, Zhang L J, Xiao L T and Jia S T 2023 *Opt. Express* **31** 19909
[29] Ćuk S M, Radonjić M, Krmpot A J, Nikolić S N, Grujić Z D and Jelenković B M 2010 *Phys. Rev. A* **82** 063802
[30] Wang B W, Xiu L W, Xiang T, Li G and Zhang H 2023 *Acta Opt. Sin.* **43** 246 (in Chinese)
[31] Ma H T, Liu Z J, Zhou P, Wang X L, Ma Y X and Xu X J 2010 *J. Opt.* **12** 045704
[32] Trypogeorgos D, Harte T, Bonnin A and Foot C 2013 *Opt. Express* **21** 24837
[33] Zheng Y C, Wu G, Chen Y S, Lu Y L, Li C, Wan G B and Yin R X 2023 *Rev. Sci. Instrum.* **94** 095010
[34] Zhang X W, Zhang X J, Duan Y, Zhang L D and Ni X J 2023 *Nat. Commun.* **14** 8374
[35] Allred J C, Lyman R N, Kornack T W and Romalis M V 2002 *Phys. Rev. Lett.* **89** 130801